IL NUOVO CIMENTO **44 C** (2021) 8
DOI 10.1393/ncc/i2021-21008-7

COMMUNICATIONS: SIF Congress 2020

Plasmonic and interband excitations of Au nanoparticles lead to different relaxation pathways

M. FERRERA

OptMatLab, Dipartimento di Fisica, Università di Genova - via Dodecaneso 33, I-16146, Genova, Italy

received 31 January 2021

Summary. — The *direct* assessment of the ultrafast temperature evolution of metallic nano-objects irradiated by a laser pulse is extremely challenging. The static thermo-optical response of plasmonic systems can be exploited as an effective spectroscopic tool to measure the temperature of impulsively excited systems after electrons and phonons have thermalized. This work shows measurements of the relaxation dynamics of ensembles of gold nanoparticles irradiated with laser pulses having two distinct photon energies, one falling within the interband transition spectral region, the other matching the plasmonic resonance. The dynamic response of these metallic nanoparticles depends on the energy of the exciting radiation.

1. – Introduction

The 3-dimensional electronic confinement occurring within metallic nano-objects gives rise to intriguing electronic and optical properties like the well-known localized surface plasmon resonance (LSPR) [1, 2]. In correspondence of the LSPR, a large fraction of the impinging electromagnetic energy is dissipated over the nano-objects. Interestingly, the exploitation of metallic nanoparticles (NPs) as remotely controlled nano-heaters, a discipline known as thermoplasmonics, proved instrumental in many applications across several scientific fields, like nanomedicine, biology, chemistry, solar harvesting and optofluidics [3-6].

The light-to-heat energy conversion provided by plasmonic NPs is caused by several scattering phenomena taking place within different temporal intervals elapsed from the exciting light pulse at the time $\tau = 0$ [7-10]. The out-of-equilibrium electron gas distribution generated by the laser pulse thermalizes via electron-electron collisions over the hundreds of femtosecond (fs) time scale. Within a few picoseconds (ps), the electron gas releases its energy to the ion lattice via electron-phonon interactions, leading to the

achievement of the intraparticle equilibrium condition. Finally, phonon-phonon scattering events occur over tens to hundreds of ps, resulting in the NPs thermalization with their environment.

However, understanding and modeling in detail the ultrafast relaxation dynamics of impulsively excited NPs is challenging [11-15] since many parameters come into play, such as the characteristics of the exciting light pulse [16, 17], numerous properties of the NPs [18-22] and those of the surrounding environment [23].

Experimentally, time-resolved optical and electronic spectroscopies have proven to be effective tools to investigate the complex relaxation mechanisms in plasmonic nanosystems and to provide pieces of information which have been cast into the general picture described above [23-28]. Moreover, pump-probe spectroscopic techniques have recently been exploited for the experimental assessment of the electron and lattice temperatures dynamics within plasmonic systems [29-31], which has typically always been evaluated indirectly [32, 33].

Recent results demonstrated that the comparison between the static thermo-optical response of metallic NPs with their dynamic counterpart can be exploited to efficiently discern between the optical fingerprint of off-equilibrium and equilibrium of plasmonic systems. Moreover, the static response can be used as a thermometric calibration scale for the ultrafast relaxation dynamics of metallic NPs [29].

By following the same approach presented in ref. [29], it is demonstrated here that this method is independent of the energy used to excite the plasmonic system and, hence, from the physical phenomenon exploited to generate heat within metallic NPs. To this aim, in this paper the static thermo-optical response of plasmonic gold (Au) NPs is compared with the dynamic optical response probed after pumping the system at two different energies, *i.e.*, within the interband spectral region and overlapping the LSPR of Au NPs (fig. 1(a)). In both cases, the static response can be used as an effective thermometric scale for the *direct* assessment of the ultrafast temperature evolution of Au NPs after the intraparticle equilibrium condition is achieved.

2. – Experimental

2˙1. *Au plasmonic array.* – An ordered array of densely packed Au NPs was fabricated via molecular beam epitaxy in a high-vacuum (HV) chamber ($P_{base} \approx 10^{-9}$ mbar),

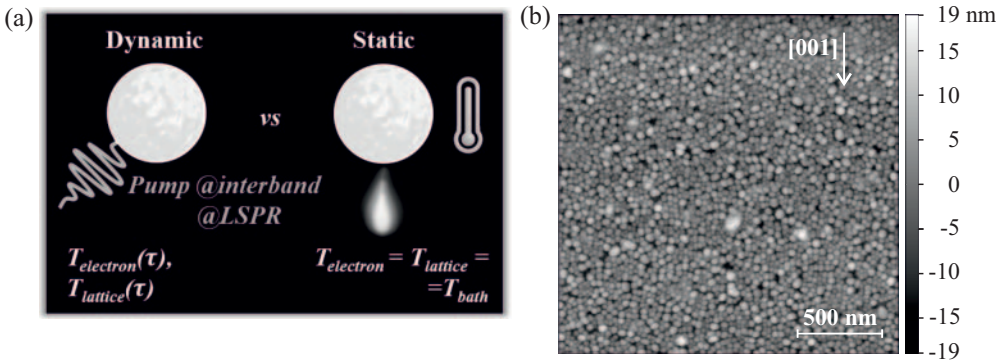

Fig. 1. – (a) Schematic representation of the presented work. (b) Atomic-force microscopy image of the two-dimensional plasmonic array: Au NPs chains are elongated along the nanogrooves of LiF substrate ([001] direction). The image size is 2×2 μm^2.

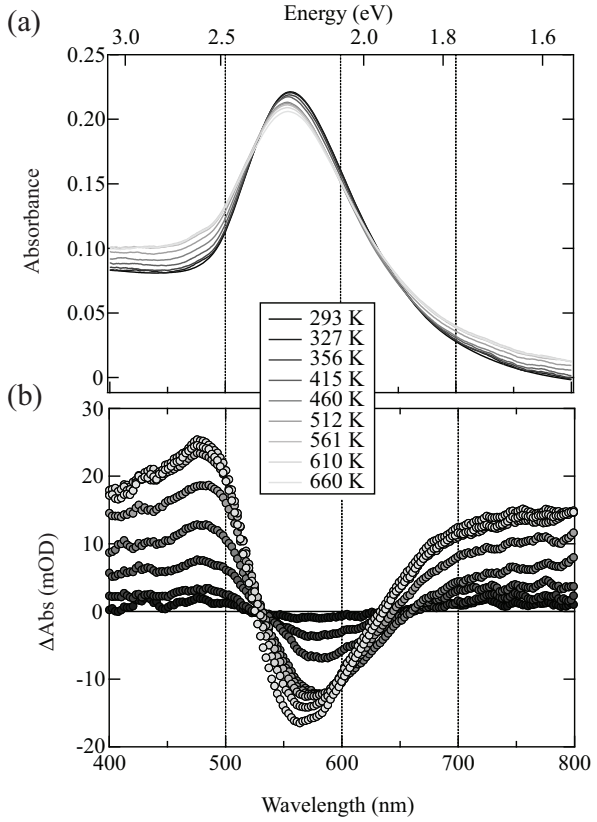

Fig. 2. – (a) Static thermo-optical response of Au NPs array. The absorbance spectra are shown for T_{bath} varying within 293–660 K temperature interval. (b) Differential-absorbance spectra, $\Delta\mathrm{Abs}(T_{bath})$ relative to the absorbance spectrum acquired at 293 K, calculated from experimental curves of graph (a) [29].

following the same procedure already detailed in previous works [29, 34-36]. Chains of Au NPs, with a mean NP size between 20 and 25 nm, elongated along the nanogrooves of a pre-nanopatterned and transparent LiF(110) substrate (Crystec GmbH), are shown in the atomic-force microscopy image of fig. 1(b). The areal density of the array is about 800 ± 100 NPs/μm^2 [29].

2˙2. *Static thermo-optical response.* – The sample was mounted onto a heating stage into a HV chamber designed for *in situ* transmittance spectroscopy [29,37]. White light, linearly polarized along the NP chains, was sent through a stress-free optical viewport onto the sample. The transmitted light passed trough a second viewport and it was collected by a spectrometer (Ocean Optics USB2000+) within the VIS-NIR spectral range (400–800 nm). Temperature-dependent transmittance spectra were collected during a cooling ramp from 660 K to room temperature (RT). By approaching RT, liquid nitrogen was used in order to speed the cooling rate and prevent the sticking of any spurious contaminant to NPs surface.

The fabricated plasmonic array exhibits LSPR at $\lambda \approx 560$ nm, corresponding to the wavelength of the maximum of the absorbance spectra in the graph of fig. 2(a). The

plasmonic peak features are determined by the electromagnetic coupling effects which arise among the NPs of the array, such that the absorbance spectrum is the result of the collective behavior of the system.

2˙3. *Dynamic optical response.* – For transient absorbance spectroscopy (TAS) experiments, a femtosecond laser system, described in detail in previous works [29, 31, 38], generated the pulses for exciting/heating the plasmonic array and probing its ultrafast optical response. Two experiments characterized by different photon energies of the pump were performed. In the first case, the pulse was set at a wavelength of 410 nm, above the threshold of Au interband transitions, while, in the second case, a wavelength of 570 nm was chosen to match the LSPR of Au NPs. The pump fluences were $F = 4 \pm 2$ J/m^2 at 410 nm and $F = 2 \pm 1$ J/m^2 at 570 nm. These fluence values are below the threshold of laser-induced permanent variation of morphology of Au NPs [17, 29]. The dynamic spectra were collected using a white light supercontinuum (SC) pulse as the probe (350–800 nm) by varying its optical path to change the time delay from the pump.

3. – Results and discussion

Figure 2(a) shows the static thermo-optical response of plasmonic Au NPs in the temperature interval 293–660 K (black to light grey curves). As already pointed out in ref. [29], the temperature increase induces a broadening of the absorbance spectra along with a loss of intensity, assigned to plasmon bleaching (PB), caused by the increased phonon population. From the curves of fig. 2(a), the differential absorbance spectra shown in fig. 2(b) were calculated as $\Delta\text{Abs}(T_{bath}) = \text{Abs}(T_{bath}) - \text{Abs}(293\text{ K})$: the PB corresponds to the negative peak in the 530–650 nm spectral window, while positive features are a fingerprint of phonon-induced absorption (PIA) due to the broadening of the resonance peak with increasing T_{bath}. In addition, the higher temperature increases the intensities of both PB and PIA spectral features, along with a redshift of PB minimum until 415 K. From this temperature onward, the PB peak undergoes a blueshift. In ref. [29], the temperature-dependent trend of PB peak was assigned to the result of two competing mechanisms induced by the heating of Au NPs, *i.e.*, the red-shift of LSPR caused by the interband transitions spectral smearing along with the blue-shift of the plasma frequency [21].

Concerning the dynamic response, fig. 3(a) shows the tridimensional plots of TAS measurements for pump wavelengths (λ_{pump}) respectively falling within the interband spectral region of Au NPs, $\lambda_{pump} = 410$ nm (upper graph), and matching the LSPR of the plasmonic array, $\lambda_{pump} = 570$ nm (lower graph). The z-axis, ΔAbs, represents the difference between the absorbance of the excited and the unperturbed system. For every time delay (y-axis) a corresponding TAS spectrum was acquired by the white light SC probe within the wavelength range 400–800 nm (x-axis). The TAS spectra were acquired from $\tau = 0$ to the maximum temporal delay of 300 ps. For both exciting energies, the laser pulse induces a rapid increase of the intensities of both the positive (PIA) and negative (PB) features in the graphs. The intensities of the two features at different λ_{pump} are very similar. Indeed, the pump fluences at both wavelengths were chosen to be inversely proportional to the corresponding absorption cross-section, thereby making the energy deposited in the nanoparticles as similar as possible. Then, both the PB and PIA intensities gradually decrease in time as a consequence of energy dissipation mechanisms mentioned above, until, at longer time delays, the plasmonic

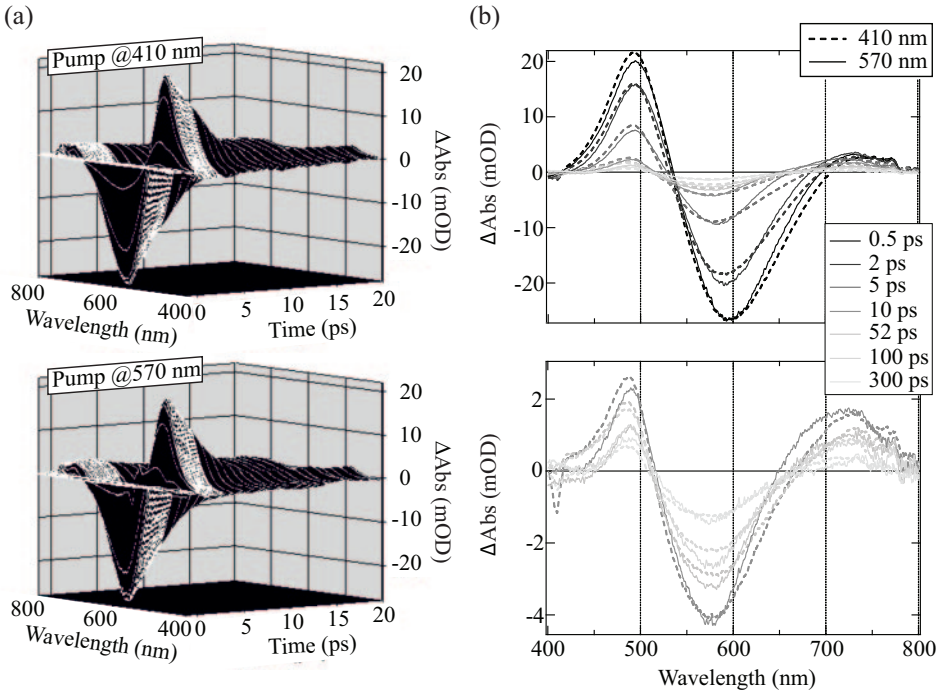

Fig. 3. – (a) Tridimensional plots of TAS data for $\lambda_{pump} = 410$ nm within the interband spectral region (upper graph) and $\lambda_{pump} = 570$ nm corresponding to LSPR of Au NPs (lower graph). To better appreciate the dynamics at lower time delays, data are shown in the temporal range 0–20 ps. The probe wavelength ranges from 400 nm to 800 nm. (b) Comparison of transient-absorbance spectra extracted at selected time delays from panel (a) between $\lambda_{pump} = 410$ nm (dashed lines) [29] and $\lambda_{pump} = 570$ nm (solid lines). The lower graph is a zoom of the upper graph to discriminate among the spectra at longer time delays (10–300 ps).

array cools down to RT [8, 14, 25, 29, 31]. To better elucidate the difference between the two sets of data obtained by pumping Au NPs at 410 nm and 570 nm, the TAS spectra were overlapped at selected time delays ranging from 0.5 ps to 300 ps (fig. 3(b)). The continuous (dashed) curves correspond to $\lambda_{pump} = 570$ nm ($\lambda_{pump} = 410$ nm). The general shape of the curves is very similar to the differential absorbance spectra as a function of T_{bath} extracted from static measurements, as reported in fig. 2(b). In ΔAbs(τ) spectra, the PB minimum is at $\lambda \approx 600$ nm, while PIA features can be observed at $\lambda \approx$490 nm and $\lambda > 700$ nm. Moreover, the spectral position of PB peak blue-shifts for increasing τ, getting closer to static PB wavelengths at longer delays. By deeply looking at the spectra, it can be noticed that the pump energy has an impact in influencing some of the characteristics of the main spectral features in the graphs. For shorter time delays (upper graph of fig. 3(b)), the TAS spectra corresponding to $\lambda_{pump} = 570$ nm if compared with those obtained for $\lambda_{pump} = 410$ nm show a narrower and slightly more intense PB peak, while the PIA peak within the low-wavelengths range is weaker. These differences are still present for longer time delays (lower graph of fig. 3(b)), even if they are much less pronounced and progressively fade away, until about 100 ps when the dynamics of the two datasets converges.

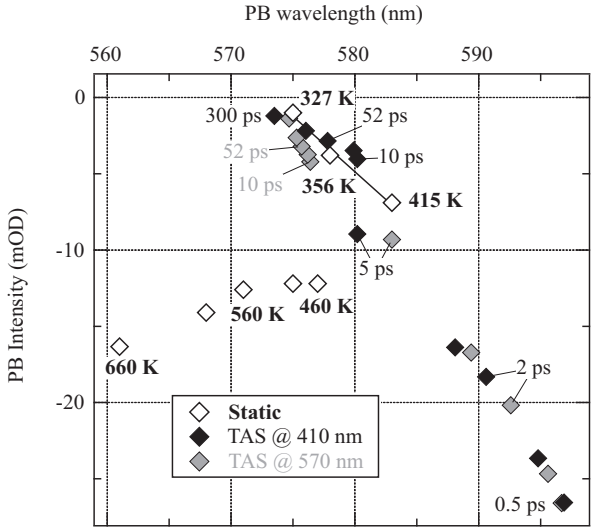

Fig. 4. – Plot of PB-peak intensity *vs.* PB-peak wavelength extracted from the static $\Delta\text{Abs}(T_{bath})$ spectra of fig. 2(b) (white diamonds) [29] and from the dynamic $\Delta\text{Abs}(\tau)$ spectra of fig. 3(b), for both $\lambda_{pump} = 410$ nm (black diamonds) [29] and $\lambda_{pump} = 570$ nm (white diamonds). The TAS data start overlapping the static ones at delays longer than $\tau \approx$10 ps. The solid black line corresponds to a linear fit of the low-T_{bath} static data (327–415 K).

By following the same procedure presented in ref. [29], in the graph of fig. 4 the PB-minimum intensity as a function of the corresponding wavelength was reported for both static (white diamonds) and TAS data (black diamonds for $\lambda_{pump} = 410$ nm and grey diamonds for $\lambda_{pump} = 570$ nm). At ultrashort time delays, none of high-T_{bath} static data can appropriately reproduce the experimental points extracted from TAS measurements, since these last ones represent the out-of-equilibrium conditions of Au NPs induced by the pump pulse within the first picoseconds [29]. For longer delays, the TAS datasets gradually approach the static markers, until the dynamic optical response starts overlapping with the static one at $\tau \approx 10$ ps and, then, it approximately follows the same trend of static data until 300 ps. The convergence between the static and dynamic optical properties can be exploited as a fingerprint of the achievement of the intraparticle equilibrium condition and offers the possibility to exploit the static data for the *direct* assessment of the temperature evolution with time of impulsively excited metallic NPs after the equilibration of electronic and lattice temperatures. By orthogonally projecting the dynamic data on the continuous black line, which corresponds to the linear fit of the low-T_{bath} static points, it was evaluated that at $\tau = 10$ ps the plasmonic array has a temperature of about 383 K for $\lambda_{pump} = 410$ nm [29] and 348 K for $\lambda_{pump} = 570$ nm. At longer delays, the temperatures reached by the plasmonic array excited at different energies become similar, until approximately becoming the same at $\tau \approx 100$ ps. From then onward, the metallic NPs ensemble cools down to RT.

Regarding the differences between the TAS datasets acquired at distinct λ_{pump} that emerge from figs. 3 and 4, several mechanisms dependent on the excitation energy can concomitantly influence the dynamic response of Au NPs, as pointed out in previous works [16, 17, 29, 31, 39]. Firstly, the pump pulse fluence affects the amount of generated hot electrons and, consequently, the dynamics of the electron and lattice tempera-

tures of metallic NPs [29]. Moreover, the same pump fluence delivered at different laser energies may affect the hot electrons distribution within the NPs at ultrashort time delays [17, 40, 41]. Irradiation of Au NPs within the interband spectral range, which in this case corresponds to $\lambda_{pump} = 410$ nm, promotes hot electrons generation throughout the NP volume, with a consequent homogeneous heating of the entire metallic nano-object. Alternatively, by exciting the system at $\lambda_{pump} = 570$ nm, which matches the LSPR of the fabricated Au NPs array, hot electrons at ultrashort time delays are spatially confined within the electromagnetic hot-spots. Indeed, under resonant condition, electromagnetic interactions between neighboring NPs affect the near-field intensity distribution at the NP surface, which reaches a maximum value in proximity of the interparticle gap [17].

Interestingly, it has also been demonstrated that interband transitions are more efficient in generating hot carriers than LSPR, which produces a lower number of higher kinetic energy carriers [16, 39]. All these observations constitute a rich background to further investigate the differences that arise into the dynamic optical response of metallic NPs excited at distinct pump energies and may help to shed light on the small variations between the two datasets that are present also at longer delays.

Nevertheless, the λ_{pump}-dependent variations between the two datasets do not affect the main result, *i.e.*, the *direct* evaluation by means of spectroscopic tools of the ultrafast temperature dynamics of plasmonic systems after the thermodynamic equilibration between the electron and lattice temperatures.

4. – Conclusion

Summarizing, this work demonstrates that, independently of the energy used to excite a plasmonic system, the static thermo-optical response of metallic NPs is an effective experimental tool to estimate the NPs temperature evolution with time after an impulsive excitation [29]. To this aim, the static T_{bath}-dependent optical properties of a closely packed array of Au NPs achieved by means of *in situ* transmittance spectroscopy was compared with its dynamic optical response, obtained by TAS. The TAS experiments were carried out by selecting two distinct λ_{pump}, namely at $\lambda_{pump} = 410$ nm, which falls within the interband spectral region, and at $\lambda_{pump} = 570$ nm, which matches the LSPR of Au NPs. Despite the λ_{pump}-dependent discrepancies observed between the two dynamic datasets, which gradually fade away at longer delays, static data can be used as a thermometric calibration scale of ultrafast processes within metallic nano-objects after electrons and phonons have thermalized, $\tau \approx 10$ ps in this case. From then onward, it is possible to follow the cooling down of the plasmonic array by *directly* assessing its temperature at the desired time delay.

* * *

The author acknowledges the OptMatLab group at the Physics Department-University of Genova, Francesco Bisio (CNR-SPIN), Maurizio Canepa (Dipartimento di Fisica, Università di Genova), Lorenzo Mattera (Dipartimento di Fisica,Università di Genova), Michele Magnozzi (Dipartimento di Fisica, Università di Genova; INFN, Sezione di Genova), Maria Sygletou (Dipartimento di Fisica, Università di Genova); people from the EuroFEL Support Laboratory (EFSL, ISM-CNR) in Rome, Daniele Catone (CNR-ISM), Patrick O'Keeffe (CNR-ISM), Alessandra Paladini (CNR-ISM), Francesco Toschi (CNR-ISM); and Giuseppe della Valle (Dipartimento di Fisica, IFN-CNR, Politecnico di Milano).

REFERENCES

[1] Coronado E. A. *et al.*, *Nanoscale*, **3** (2011) 4042.
[2] Louis C. and Pluchery O., *Gold Nanoparticles for Physics, Chemistry and Biology*, (Imperial College Press, London) 2012.
[3] Baffou G., *Thermoplasmonics: Heating Metal Nanoparticules Using Light*, (Cambridge Unversity Press) 2017.
[4] Kamarudheen R. *et al.*, *ACS Nano*, **12** (2018) 8447.
[5] Baffou G. *et al.*, *Light Sci. Appl.*, **9** (2020) 108.
[6] Baffou G. *et al.*, *Nat. Mater.*, **19** (2020) 946.
[7] Hartland G. V., *Phys. Chem. Chem. Phys.*, **6** (2004) 5263.
[8] Hartland G. V., *Chem. Rev.*, **111** (2011) 3858.
[9] Brongersma M. L. *et al.*, *Nat. Nanotechnol.*, **10** (2015) 25.
[10] Pustovalov V. K., *RSC Adv.*, **6** (2016) 81266.
[11] Pustovalov V. K., *RSC Adv.*, **4** (2014) 55760.
[12] Stoll T., *Eur. Phys. J. B*, **87** (2014) 260.
[13] Saavedra, J. R. M. *et al.*, *ACS Photonics*, **3** (2016) 1637.
[14] Brown A. M. *et al.*, *Phys. Rev. Lett.*, **118** (2017) 087401.
[15] Block A. *et al.*, *Sci. Adv.*, **5** (2019) eaav8965.
[16] Zhao J.. *et al.*, *ACS Cent. Sci.*, **3** (2017) 482.
[17] Magnozzi M. *et al.*, *J. Phys. Chem. C*, **123** (2019) 16943.
[18] Halté V. *et al.*, *Appl. Phys. Lett.*, **75** (1999) 3799.
[19] Manjavacas A. *et al.*, *ACS Nano*, **8** (2014) 7630.
[20] Harutyunyan H. *et al.*, *Nat. Nanotechnol.*, **10** (2015) 770.
[21] Magnozzi M. *et al.*, *Nanoscale*, **11** (2019) 1140.
[22] Ferrera M. *et al.*, *Phys. Rev. Mater.*, **3** (2019) 105201.
[23] Stoll T. *et al.*, *J. Phys. Chem. C*, **119** (2015) 12757.
[24] Guillet Y. *et al.*, *Phys. Rev. B*, **79** (2009) 195432.
[25] Wang X. *et al.*, *J. Phys. Chem. C*, **119** (2015) 7416.
[26] Hobbs R. G. *et al.*, *Nano Lett.*, **17** (2017) 6069.
[27] Lietard A. *et al.*, *Nat. Commun.*, **9** (2018) 891.
[28] Ortolani M. *et al.*, *Phys. Rev. B*, **99** (2019) 035435.
[29] Ferrera M. *et al.*, *ACS Photonics*, **7** (2020) 959.
[30] Jollans T. *et al.*, *J. Phys. Chem. A*, **124** (2020) 6968.
[31] Catone D. *et al.*, *Nanotechnology*, **32** (2020) 025703.
[32] Van de Broek B. *et al.*, *Small*, **7** (2011) 2498.
[33] Plech A. *et al.*, *Nanoscale*, **9** (2017) 17284.
[34] Sugawara A. and Mae K., *J. Vac. Sci. Technol. B: Microelectron. Process. Phenom.*, **23** (2005) 443.
[35] Proietti Zaccaria R. *et al.*, *ACS Appl. Mater. Interfaces*, **8** (2016) 8024.
[36] Magnozzi M. *et al.*, *J. Phys.: Conf. Ser.*, **1226** (2019) 012014.
[37] Ferrera M. *et al.*, *J. Phys. Chem. C*, **124** (2020) 17204.
[38] Fratoddi I. *et al.*, *J. Colloid Interface Sci.*, **513** (2018) 10.
[39] Bernardi M., *Nat. Commun.*, **6** (2015) 7044.
[40] Schirato A. *et al.*, *Nat. Photonics*, **14** (2020) 723.
[41] Schirato A. *et al.*, *Nano Lett.*, **21** (2021) 1345.